water

MDPI

Technical Note

Hazard Zonation and Risk Assessment of a Debris Flow under Different Rainfall Condition in Wudu District, Gansu Province, Northwest China

Shuai Zhang [1,2,3], Ping Sun [1,2,3,*], Yanlin Zhang [4], Jian Ren [1,2,3] and Haojie Wang [1,2,3]

[1] Institute of Geomechanics, Chinese Academy of Geological Sciences, Beijing 100081, China
[2] Observation and Research Station of Geological Disaster in Baoji, Ministry of Natural Resources, Baoji 721001, China
[3] Key Laboratory of Active Tectonics and Geological Safety, Ministry of Natural Resources, Beijing 100081, China
[4] Geological Survey of Gansu Province, Lanzhou 730000, China
* Correspondence: sunpingcgs@foxmail.com; Tel.: +86-10-8881-5112

Abstract: Debris flows induced by heavy rainfall are a major threat in Northwest and Southwest China, due to its abrupt occurrence and long runout. In light of this, this work presents the runout simulation and risk assessment of the Boshuigou debris flow under different rainfall conditions in Wudu district, Gansu Province, Northwest China. Based on field reconnaissance, the geomorphological feature and main source of the Boshuigou debris flow were described. With the application of the FLO-2D simulation, the potential flow depth and flow extent of the Boshuigou debris flow under 100-year return-period rainfall and 50-year return-period rainfall were calculated. The maximum flow velocities of the Boshuigou debris flow under the 100-year return-period rainfall and 50-year return-period rainfall were 5.46 and 5.18 m/s, respectively. Accordingly, the maximum flow depths were 5.85 and 5.57 m. Then, the hazard zonation was conducted in combination of the construction and other properties within the potential impact zone, and the risk assessment of the Boshuigou debris flow under the 100-year return-period rainfall and 50-year return-period rainfall was finally completed. This work presents a method for debris flow risk assessment considering the solid source and water flow, which can provide a basic reference for mitigation and reduction of geohazards induced by torrential rainfall.

Keywords: debris flow; geomorphological feature; hazard zonation; risk assessment

Citation: Zhang, S.; Sun, P.; Zhang, Y.; Ren, J.; Wang, H. Hazard Zonation and Risk Assessment of a Debris Flow under Different Rainfall Condition in Wudu District, Gansu Province, Northwest China. *Water* **2022**, *14*, 2680. https://doi.org/10.3390/w14172680

Academic Editor: Stefano Luigi Gariano

Received: 12 June 2022
Accepted: 26 August 2022
Published: 29 August 2022

1. Introduction

Rainfall-induced debris flow frequently occurs worldwide and results in catastrophic damage to society [1–6]. In March 2012, a >100-year return period rainfall event in an arid region triggered a few debris and mud flows resulting in severe damage and destruction to several small villages along the Camina and Tarapaca valleys in northern Chile [7]. On 12 July 2008, two large debris flows were triggered following a brief period of intense rainfall in Southern Sierra Nevada, CA, United States of America and resulted in catastrophic causalities and destruction [8]. On the night of 31 March 2017, a rainfall-induced landslide event with more than 600 shallow landslides and debris flows was triggered in Mocoa, southern Colombia, and 333 people were killed [9]. On 3 July 2021, the Atami debris flow in Shizuoka, Japan was triggered following persistent precipitation and claimed 26 fatalities, 1 missing, and 28 injuries [10]. In a similar vein, rainfall-induced debris flow is a major threat in Northwest and Southwest China due to their fragile ecological environment. On 7 August 2010, a giant mudflow occurred in Zhouqu, Gansu, Northwest China and killed at least 1467 people [11]. Again, on 22 July 2013, one day after the Ms 6.6 Minxian earthquake, a debris flow (Dagou debris flow) occurred in Tianshui, Gansu, Northwest

China and destroyed 137 houses [12]. To effectively evaluate the runout and impact zone of rainfall-induce debris flow, the formation mechanism and runout assessment/prediction of debris flow were conducted on catastrophic debris flow events [13,14]. For the runout assessment/prediction, numerical simulation is an effective way, and several simulation methods have been developed [3,15–17]. Several famous software simulations (RAMMS, MASSFLOW, Debris-2D, FLO-2D) have been widely applied in the runout simulation in previous study worldwide [18–22]. FLO-2D is a professional software developed for flow simulation of flood and debris flow and can veritably simulate and reflect the rheological state during flow motion [23–26]. The aforementioned studies well simulate the flow process, deposition feature and potential runout, but a few research studies have been conducted on risk assessment considering the potential runout and impact zone, especially under different return-period rainfalls.

In this light, this work aims to present the runout estimation and risk assessment of a debris flow frequently occurring in Wudu district, Gansu Province, Northwest China. To accurately obtain the total solid source (including landslide deposits, collapse deposits, and gully deposits) of the Boshuigou debris flow, a detailed field survey was conducted. Then, the fluid feature of the debris flow under different rainfall conditions was investigated. The FLO-2D numerical simulation enables the assessment of the potential flow extent and impact zone of the Boshuigou debris flow under the 100-year return-period rainfall and 50-year return-period rainfall. On this basis, the hazard zonation was conducted considering the flow velocity, flow depth, and frequency of the debris flow under different rainfall conditions. Finally, the risk assessment of the Boshuigou debris flow under the 100-year return-period rainfall and 50-year return-period rainfall was completed in combination of the properties (including population, construction, land use, road, and other information) within the flow extent.

2. Site Features

2.1. Geomorphological and Topographic Features

The Boshuigou debris flow is located in Wudu district, Longnan city, Southwest Gansu (Figure 1a). This region is situated in the transition zone from the second step to the third step on the Chinese continent and the intersection area of the Qinba mountain region, the Qinghai-Tibet Plateau, and the Loess Plateau. Wudu district is characterized by interleaving terrain of precipitous mountains and valley basins with a general terrain of high in the northwest and low in the southeast (Figure 1b). Correspondingly, the geomorphic unit of the study area and its vicinity can be classified as river valley landform (river terrace and alluvial–proluvial fan) and middle-high altitude mountain [3]. The river terrace is distributed along the Bailong River and its tributary, and the alluvial–proluvial fan is mainly observed in the Beiyu River. The middle-high altitude mountain is mainly distributed on both sides of the Bailong River. The left side (north side) of the Bailong River is constituted by the Devonian and Silurian phyllite; the right side (south side) of the Bailong River comprises the Carboniferous limestone.

The Boshuigou debris flow with a fan shape is the primary tributary of the Bailong River (Figure 2a). The basin area of the Boshuigou debris flow is 10.5 km^2, and the gullies are well developed. The relative relief is 1910 m with a maximum and minimum elevation of approximately 2910 and 1000 m (Figure 2b), and the length of the largest gully is approximately 3.53 km with a gradient of 126‰. At least four major gullies are developed at the upper stream with a density of 2.48 km/km^2. The upper part of the gullies is characterized by a "V" shape with a width of 3–10 m and slope gradient of 30–50°, and the lower part of the gullies is characterized by a "U" shape with a width of 15–30 m and slope gradient of 25–40°. The high relative relief and gradient and the well-developed gullies provide favorable topographic condition for debris flow occurrence.

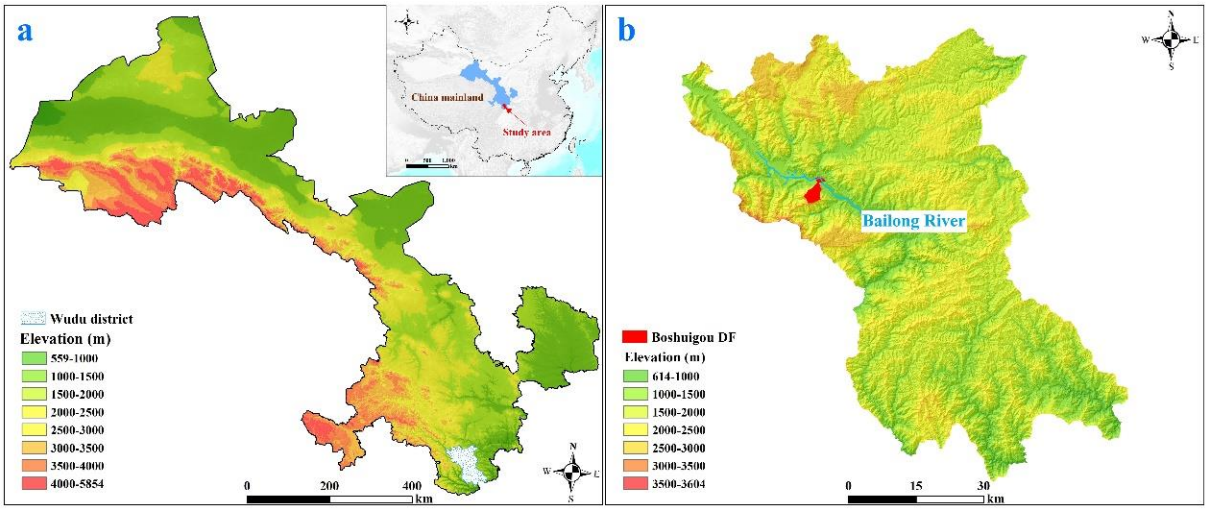

Figure 1. Location (**a**) and topography (**b**) of the Boshuigou debris flow and its vicinity.

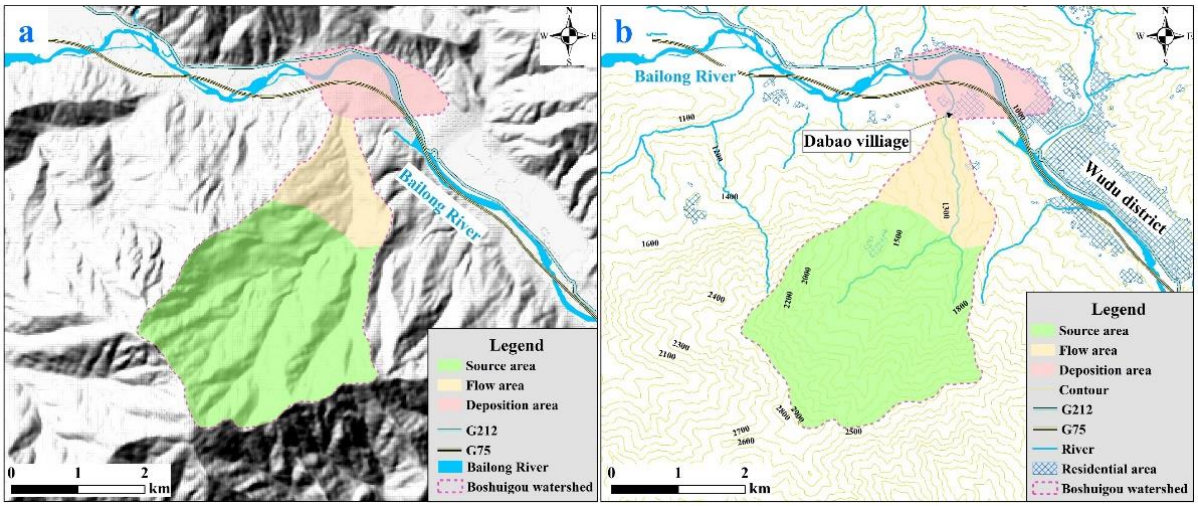

Figure 2. Panoramic (**a**) and planar view (**b**) of the Boshuigou debris flow. G212 and G75 are abbreviations of the Lanzhou–Longbang Highway and Lanzhou–Haikou Expressway, respectively.

2.2. Geological Setting and Precipitation Condition

The outcropped strata of the study area and its vicinity consist of the Silurian phyllite and slate, the Carboniferous argillaceous limestone and siliceous limestone, and the Quaternary loess (Upper Pleistocene), colluvial deposit, residual deposit, alluvial–proluvial deposit and fluvial deposit (Figure 3) [27–29]. The Silurian phyllite and slate are mainly outcropped at the debris flow source area and weathered phyllite and slate pieces of size between 5 and 10 cm can be observed in the field. Interbedded layers of slate and phyllite with different weathering resistance provide a favorable lithology condition for debris flow source. The Carboniferous argillaceous limestone and siliceous limestone are the major sources of the coarse content of the debris flow, as they are not vulnerable to weathering, and collapses can be observed at the steep area. The Quaternary loess is mainly distributed at the upper stream, and shallow slope failures occur occasionally. The colluvial deposit and residual deposit are mainly derived from the weather slate and phyllite. The alluvial–proluvial deposit with a fan shape at the watershed outlet is the result from historical debris flow, and no obvious rhythmic bedding can be observed. The fluvial deposit is only located at the watershed outlet and belongs to the river terrace of the Bailong River.

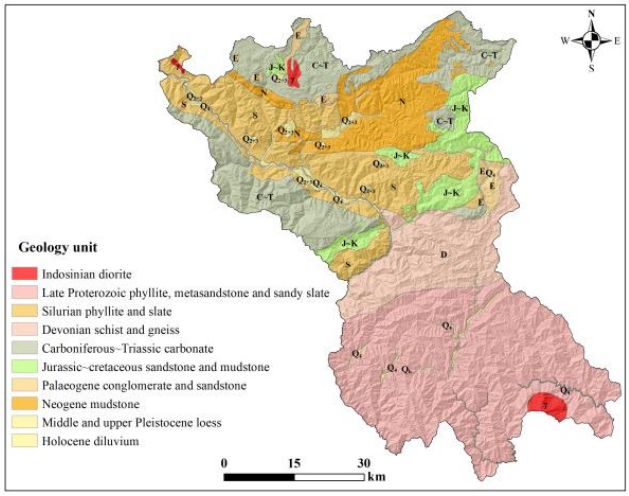

Figure 3. Geological setting of the study area. The geological map is derived from the local government.

The study area is situated at the transition zone from the subtropical monsoon climate to the warm temperate humid monsoon climate. Affected by steep topography, the climate varies vertically, and the precipitation increases with an increase in elevation. Based on the meteorological data (1980 to 2020) from the local government, the average annual precipitation is 483 mm, and the maximum and minimum annual precipitation are 270 mm (1997) and 774 mm (2020), respectively (Figure 4). The cumulative precipitation in 2020 is also the largest ever recorded in this area. The day with daily precipitation higher than 0.1 mm is 96 per year, and the cumulative precipitation (235.6 mm) in the summer season (June to August) accounts for approximately 49% of the average annual precipitation. The maximum daily precipitation of 79.2 mm was recorded on 7 August 2017 (Figure 4). The temporarily uneven distribution of precipitation and high concentration from May to September offer favorable hydrological conditions for rainfall-induced geohazard occurrence.

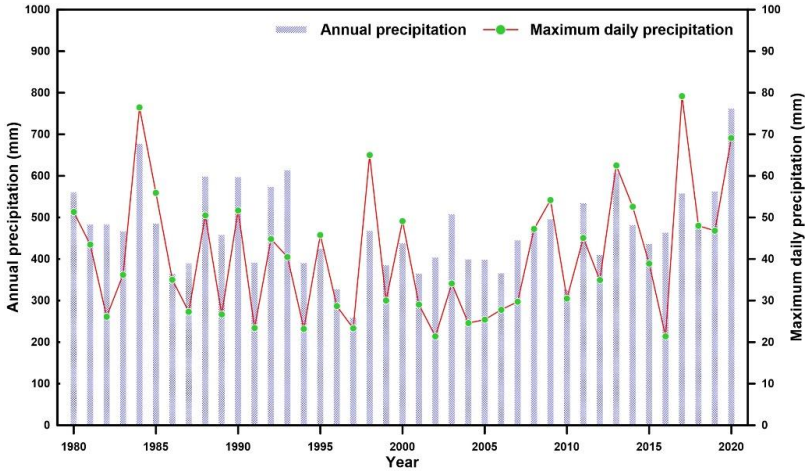

Figure 4. Annual precipitation and maximum daily precipitation of the study area from 1980 to 2020.

3. Characteristics and Source of the Boshuigou Debris Flow

3.1. Formation Feature

Based on the topographic feature and potential motion feature, the Boshuigou debris flow can be classified as the source area, flow area and deposition area (Figure 2). The source area with an area of approximately 7.34 km^2 consists of a water source and solid source. The area of the flow area and deposition area are 1.57 and 1.50 km^2, respectively. The water source area is located at the well-forested south part of the watershed, and limestone is outcropped. The solid source is north to the water source area, and the bedrock

is exposed. Landslides and rock collapses can be observed, and down-cutting erosion is well developed. The steep topography and strong hydrodynamic condition (Figure 2a) lay the foundation for debris flow occurrence. The flow area is located downstream with a length of 1.12 km. The slope gradient of both sides of the flow area is approximately 30°, and the deposits of this area account for 10–15% of the total debris flow source. The deposition area is located at the watershed outlet, and the deposition fan is 0.623 km^2 with a length of 790 m and width of 950 m. The relatively flat deposition area is densely inhabited (Figure 2b). The Dabao village, national highway (G212), and expressway (G75) are situated at the deposition area.

The Boshuigou debris flow is a typical V-shaped hydrodynamic debris flow in degenerating stage judged from the deposition fan and outburst history. Based on a detailed field survey, the deposition fan of the Boshuigou debris flow with an area of 0.623 km^2 consists of at least two stages. The slope gradient of the deposition fan is 71‰, and maximum thickness is over 10 m. Due to the steep topography at the source area, high gradient of the flow path, and abundant source deposits, the Boshuigou debris flow is characterized by rapid runoff and a large flow amount. Based on the consultation with local residents and the government, the debris flow occurs two to three times every year. The size of the deposit decreases along the flow path. Based on our preliminary tests of the grain size of deposits in the flow path, the masses of deposit with sizes larger than 20 mm, 2–20 mm, and smaller than 2 mm account for 43%, 41% and 16%, respectively.

3.2. Main Source of the Debris Flow

Due to steep topography of the study area and high weathering in phyllite (observed during field survey), slope failures are well developed in the Boshuigou debris flow, which serve as the solid source of the debris flow (in addition to the large amounts of loose Quaternary deposits). Based on the field investigation, six landslides with a total area of 0.70 km^2 and a total volume of 2.7×10^6 m^3 are observed in the Boshuigou watershed (Figure 5a), and the sliding mass mainly consists of weathering phyllite, talus material, and residual deposit. The uppermost area of the debris flow is an escarpment with the limestone, and more than 10 rock collapses are developed with the influence of the 2008 Wenchuan earthquake and strong weathering. The total area and volume of the rock collapses are 0.3 km^2 and 0.25×10^6 m^3 (Figure 5b,c). In addition, slope erosion of the weathered loose materials with a thickness of approximately 0.2 m at slope also contributes to the source of the debris flow (Figure 5d). The deposits along the flow path and at the source area are another main source of the debris flow, and total volume of the deposits in the valley is estimated to be approximately 0.4×10^6 m^3 (Figure 5e,f). In addition, loose debris with a thickness of approximately 0.2 m is deposited at the slope. The total solid source of the Boshuigou debris flow is approximately 3.75×10^6 m^3.

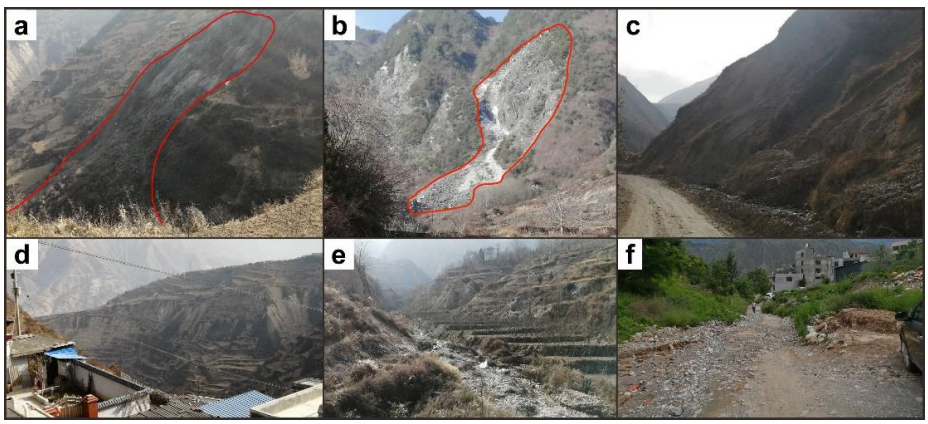

Figure 5. Main source of the Boshuigou debris flow: (**a**) landslide at the source; (**b**) rock collapse at the source; (**c**) collapse at the flow path; (**d**) slope erosion at the flow path; (**e**) deposits at the flow path; (**f**) deposits at the deposition area.

4. Flow Simulation under Different Return-Period Rainfalls

4.1. Fluid Feature of the Debris Flow

FLO-2D developed by O'Brien [23] is an effective way for debris flow simulation and has been widely applied in previous case studies [30–34]. In this work, the flow velocity and flow depth of the Boshuigou debris flow under the 100-year return-period rainfall and 50-year return-period rainfall were investigated. In the simulation, three key factors, i.e., unit weight, flow rate, and total discharge, should be considered. The calculation of the unit weight of the debris flow is calculated following an empirical equation:

$$\gamma_c = 10.6A^{0.12} \quad (1)$$

where γ_c is the unit weight of debris flow, and A is the solid source per unit (Table 1). The calculated unit weight of the Boshuigou debris flow is 16.27 kN/m^3. The unit weight of the debris flow reflects the solid content, which indicates the property of the debris flow. The Boshuigou debris flow belongs to a transition type between viscous debris flow and diluted debris flow.

Table 1. Parameters concerning the solid source in the simulation.

Parameters	Watershed Area (km^2)	Solid Source Volume (10^6 m^3)	Solid Source Per Unit (10^4 m^3/km^2)	Unit Weight (kN/m^3)
Value	10.50	3.75	35.7	16.27

The discharge of the debris flow under certain return-period rainfall is calculated with the following equation:

$$Q_D = Q_B(1 + \varphi)D \quad (2)$$

where Q_D is the discharge of the debris flow under a certain return-period rainfall, Q_B is the discharge of the water under the same return-period rainfall, φ is the coefficient calculated with Equation (3), and D is the obstructive coefficient of debris flow. In this work, the value of the obstructive coefficient is set as 1.2.

$$\varphi = \frac{\gamma_c - 10}{\gamma_H - \gamma_c} \quad (3)$$

where γ_H is the unit weight of the debris flow particle, and its value is set as 26.5 kN/m^3 in this work.

The discharge of the water under the 100-year return-period rainfall, $Q_{B(1\%)}$, is calculated using the following equation:

$$Q_{B(1\%)} = 11.2F^{0.84} \quad (4)$$

where F is the watershed area of the Boshuigou debris flow. The discharge of the water under the 50-year return-period rainfall ($Q_{B(2\%)}$) is 80% of the discharge of the water under the 100-year return-period rainfall ($Q_{B(1\%)}$). The corresponding key values of the Boshuigou debris flow are listed in Table 2.

Table 2. Key values concerning the discharge of the Boshuigou debris flow under different return-period rainfalls.

Parameters	F (km^2)	$Q_{B(1\%)}$ (m^3/s)	$Q_{B(2\%)}$ (m^3/s)	1+φ	D	$Q_{C(1\%)}$ (m^3/s)	$Q_{C(2\%)}$ (m^3/s)
Value	10.50	80.73	64.58	1.624	1.2	157.33	125.85

For the debris flow runout simulation, the flood hygrograph (discharge of water and debris flow at different time) should be input. Since no detailed hydrological information is available in this debris flow, a simplified method that has been used in previous studies

was employed in this work [19]. In this simplified method, the peak discharge is assumed to appear at one half of the total outburst duration, a third of the peak discharge is assumed to appear at two thirds of the total outburst duration, and a quarter of the peak discharge is assumed to appear at one third of the total outburst duration. Based on the outburst history of the Boshuigou debris flow, the total duration of the Boshuigou debris flow that was triggered in August 1983 under the 100-year return-period rainfall is approximately 30 min. Thus, the flood hygrographs of water and debris flow are depicted in Figure 6.

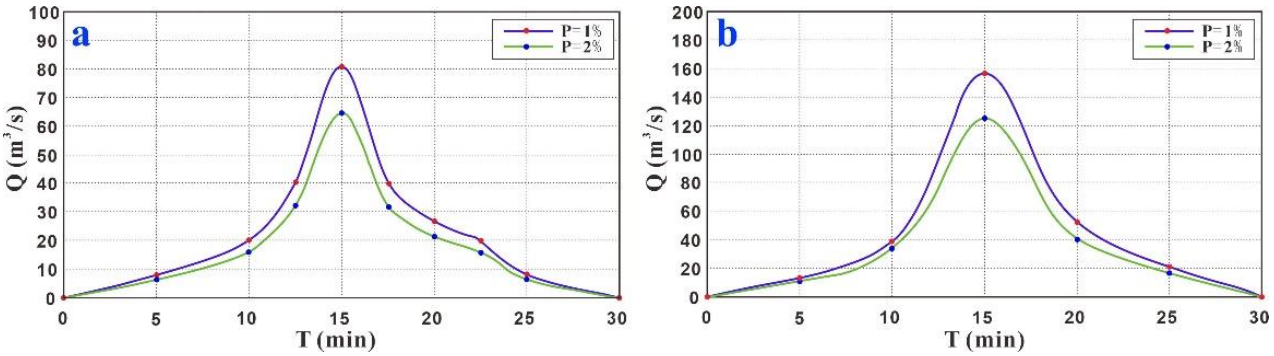

Figure 6. Flood hygrographs of water (**a**) and debris flow (**b**) under different return-period rainfalls in the Boshuigou debris flow simulation.

4.2. Key Parameters of the FLO-2D Simulation

FLO-2D is a pseudo-2D model in space that adopts depth-integrated flow equations [35]. Hyperconcentrated sediment flows are simulated considering the flow as a homogeneous (monophasic) non-linear Bingham fluid, based on an empirical quadratic rheological relation developed by O'Brien and Julien [36]. The numerical scheme and the general constitutive fluid equations adopted in the Flo-2D model can be found in FLO-2D User's Manual [23], and the total slope friction (S_f) can be calculated with the following equation:

$$S_f = \frac{\tau_B}{\rho g h} + \frac{K\mu_B V}{8\rho g h^2} + \frac{n^2 V^2}{h^{\frac{4}{3}}} \quad (5)$$

where ρ is mixture density, g is gravitational acceleration, h is flow depth, τ_B is Bingham yield stress, μ_B is Bingham viscosity, K is the laminar flow resistance coefficient, n is the pseudo-Manning resistance coefficient, which accounts for both turbulent boundary friction and internal collisional stresses, and V is depth-averaged velocity. The Bingham yield stress, the dynamic viscosity and the resistance coefficient are influenced by the sediment concentration relationships, which can be described by the following equations [23]:

$$\tau_B = \alpha_1 e^{\beta_1 C_V} \quad (6)$$

$$\mu_B = \alpha_2 e^{\beta_2 C_V} \quad (7)$$

$$n = n_t e^{\beta_1 C_V} \quad (8)$$

where α_1, β_1, α_2, and β_2 are empirical coefficients and C_V is the volumetric concentration defined by laboratory experiments [37], and n_t is the turbulent value [38].

In this work, the flow simulation is calculated with uniform square grid elements with size 5 × 5 m, and the unit weight of the Boshuigou debris flow is set as 16.27 kN/m^3. Other parameters used in the simulation of the Boshuigou Debris flow are listed in Table 3.

Table 3. Several parameters used in the FLO-2D simulation.

Parameters	K	n	α_1	β_1	α_2	β_2	C_V
Value	2280	0.15~0.25	0.00461	11.25	0.812	13.71	0.59

4.3. Simulation Result and Hazard Zonation

During the runout simulation of the Boshuigou debris flow under different rainfall conditions, the main consideration is the discharge difference resulted from different rainfalls. Different discharges of debris flow (Figure 6b) were set as input in the simulation. In this work, the flow depth and flow velocity of the Boshuigou debris flow under the 100-year return-period rainfall (p = 1%) and the 50-year return-period rainfall (p = 2%) were obtained (Figures 7 and 8). Based on the simulation results, the maximum flow depth, maximum flow velocity, maximum runout of the deposition and maximum width of the deposition of the Boshuigou debris flow under different return-period rainfalls are summarized in Table 4. The maximum flow velocities of the Boshuigou debris flow under the 100-year return-period rainfall and 50-year return-period rainfall were 5.46 and 5.18 m/s, respectively. The maximum flow depths under the 100-year return-period rainfall and 50-year return-period rainfall were 5.85 and 5.57 m. The simulation indicates that the runout extent increases with the increase in return-period rainfall, and the maximum flow depths (or deposition depth) for both conditions are less than 6.0 m. The maximum flow depth and flow velocity for each simulation appears at the flow path due to its high slope gradient and narrow flow channel. In addition, the Boshuigou debris flow passes through the residential area (Dabao Village, Figure 2) under both return-period rainfall and may cause severe damage to the residents. The debris flow under the 100-year return-period rainfall runs across the Bailong River to the opposite bank. Thus, the Bailong River has a certain possibility to be dammed under the 100-year return-period rainfall.

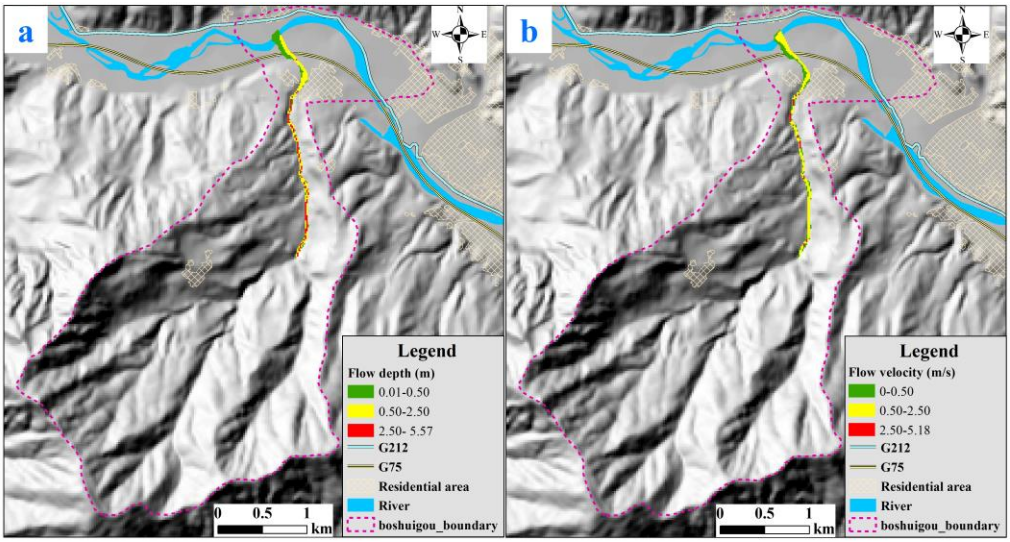

Figure 7. Flow depth (**a**) and flow velocity (**b**) of the Boshuigou debris flow under the 50-year return-period rainfall.

To evaluate the hazard caused by the debris flow, the impact intensity and recurrence period were considered. The impact intensity of the debris flow is affected by the flow depth and flow velocity, and detailed impact grade is classified based on Table 5. The hazard assessment is jointly affected by the impact intensity and recurrence period, and the hazard grade is assessed by Table 6. Based on this grade, the hazard zonation was conducted (Figure 9). The area with high hazard accounts for 57.32% of the total flow area and is concentrated on the flow path of the Boshuigou debris flow. Part of the residents and farmlands of the Dabao Village are at risk. The area with medium hazard accounts for 2.48% of the total flow area and is distributed in the valley passing through the Dabao Village. The residents and constructions near both banks are at risk. The area with low hazard accounts for 40.20% of the total flow area and is located in the southwest part of the deposition where the residential area, national highway (G75) and some farmlands are at risk. Detailed hazard zonation is depicted in Figure 9.

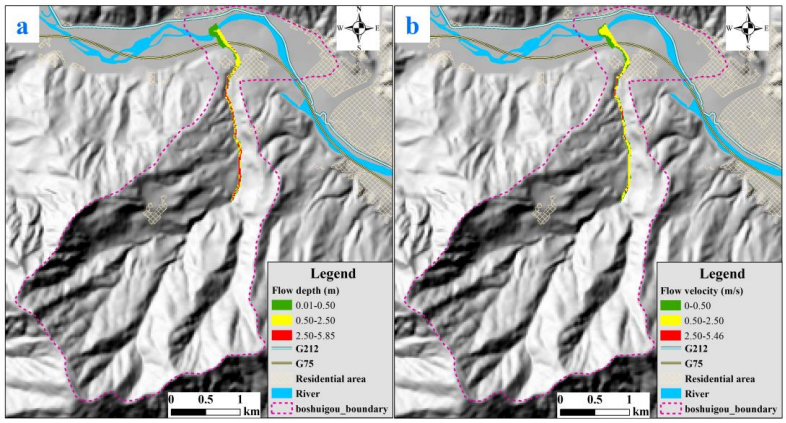

Figure 8. Flow depth (**a**) and flow velocity (**b**) of the Boshuigou debris flow under the 100-year return-period rainfall.

Table 4. Simulation result of the Boshuigou debris flow under different return-period rainfalls.

Frequency	Maximum Flow Depth (m)	Maximum Flow Velocity (m/s)	Maximum Runout of the Deposition (m)	Maximum Width of the Deposition (m)
1%	5.85	5.46	935	183
2%	5.57	5.18	880	138

Table 5. Impact grade of the debris flow.

Grade	Flow Depth (m)	Logical Relation	Flow Velocity × Flow Depth (m^2/s)
High	$H \geq 2.5$	or	$Vh \geq 2.5$
Medium	$0.5 \leq h < 2.5$	and	$0.5 \leq Vh < 2.5$
Low	$0.001 \leq h < 0.5$	and	$Vh < 0.5$

Table 6. Hazard assessment considering impact intensity and recurrence period.

Impact Grade / Recurrence Period	High	Medium	Low
100-year	High	Medium	Low
50-year	Medium	Low	Low

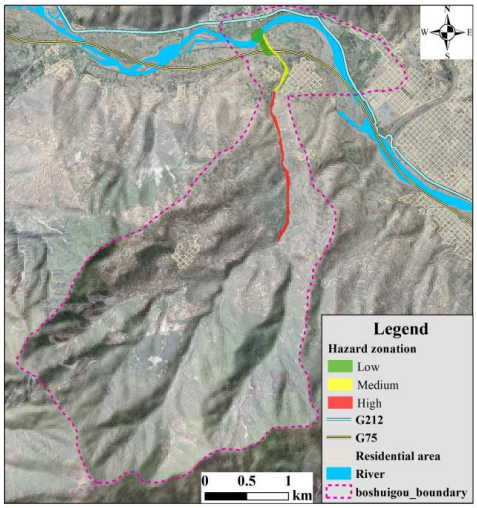

Figure 9. Hazard zonation of the Boshuigou debris flow.

5. Risk Assessment

5.1. Classification of Assessment Unit and Their Vulnerability Assessment

To quantitatively evaluate the potential loss resulting from the Boshuigou debris flow under different return-period rainfalls, the flow area was classified as 27 units based on the distribution of population, land use and roads (Figure 10), and the area, population, and properties of 27 units were calculated in detail (Table 7). Then, the potential economic loess and environmental loss were assessed and classified as three grades (not severe, severe, and serious) (Table 7).

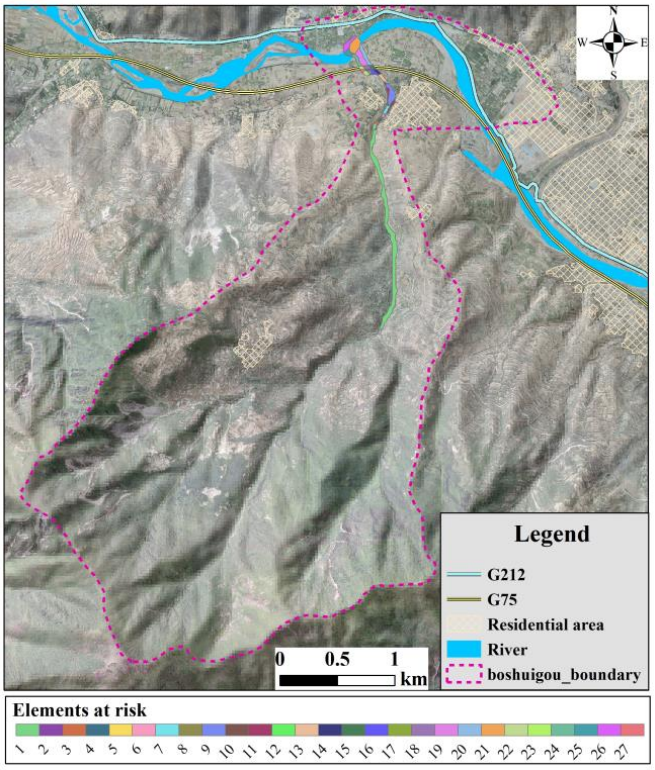

Figure 10. Detailed classification of elements at risk.

For vulnerability assessment of elements at risk, temporal and spatial probability of elements should be considered. The temporal and spatial probability of all fixed elements (such as building, road, and land) is 1.0. For the temporal and spatial probability of personnel, the duration (or probability) should be considered. The duration of personnel at residential areas and working places (such as factory, hospital, school) are 14 and 8 h, respectively, and the temporal and spatial probability are 0.58 and 0.33, respectively. Similarly, the temporal and spatial probability for open public area is 0.50. Then, the annual probability of personnel and the economy can be calculated considering the temporal and spatial probability, recurrence period, and onsite investigation. The calculated results are listed in Table 8.

5.2. Risk Assessment and Risk Zonation

The risk of debris flow incorporates its hazard and the vulnerability of elements at risk and can be jointly confirmed by the annual probability of personnel loss and annual probability of property loss. Generally, geoenvironmental condition, formation feature, outburst history, local economic situation, and damage resulting from a recent outburst should be considered to determine the risk grading standard. In this light, the risk grading standard of the Boshuigou debris flow was finalized, as shown in Table 9, and the risk assessment for 27 units was confirmed (Table 10).

Table 7. Twenty-seven units for risk assessment and their potential damage under different return-period rainfalls.

NO	Recurrence Period	Area (m^2)	Population	Properties (10^3 RMB)					Property Loss	Environmental Loss
				Construction	Land	Road	Other	Total		
1	50-year	59,962.9	0	0	730	390	0	1120	Serious	Severe
2	50-year	415.2	8	285	0	0	0	285	Serious	Not severe
3	50-year	1655.1	0	0	101	0	0	101	Not severe	Serious
4	50-year	911.7	0	0	0	0	10	10	Not severe	Not severe
5	50-year	231.4	0	0	0	23	0	23	Not severe	Serious
6	50-year	612.2	0	0	0	0	30	30	Not severe	Not severe
7	50-year	2079.5	0	0	122	0	0	122	Not severe	Serious
8	50-year	912.1	0	0	0	91	0	91	Not severe	Serious
9	50-year	8154.6	13	300	487	0	0	787	Serious	Serious
10	50-year	2612.7	73	1660	0	0	30	1690	Severe	Serious
11	50-year	2112.5	6	180	122	0	0	302	Serious	Serious
12	50-year	273.0	0	0	0	27	0	27	Not severe	Not severe
13	50-year	2482.5	4	0	162	0	50	212	Not severe	Serious
14	50-year	1798.8	3	0	0	0	50	50	Not severe	Not severe
15	50-year	1435.9	0	0	0	1250	0	1250	Serious	Severe
16	50-year	2421.1	0	0	146	0	0	146	Not severe	Serious
17	50-year	710.51	12	0	0	0	30	30	Not severe	Not severe
18	50-year	1639.7	0	0	0	1500	0	1500	Serious	Severe
19	50-year	7628.6	0	0	467	0	0	467	Not severe	Serious
20	50-year	5654.1	0	0	0	0	10	10	Not severe	Not severe
21	50-year	9433.7	0	0	0	0	10	10	Not severe	Not severe
22	100-year	1758.4	20	0	0	0	80	80	Not severe	Serious
23	100-year	1156.6	0	0	0	1250	0	1250	Serious	Severe
24	100-year	3023.8	0	0	183	0	0	183	Not severe	Serious
25	100-year	3056.9	0	0	0	0	0	0	Not severe	Not severe
26	100-year	5543.7	0	0	0	0	200	200	Not severe	Serious
27	100-year	907.2	0	0	57	0	0	57	Not severe	Serious

Table 8. Annual probability of personnel loss and property loss of all 27 units.

NO	Recurrence Period	Area (m^2)	Population	Personnel Vulnerability	Personnel Temporal and Spatial Probability	Properties (10^3 RMB)	Properties Vulnerability	Property Temporal and Spatial Probability	Annual Probability of Personnel Loss	Annual Probability of Property Loss
1	50-year	59,962.93	0.00	0.70	0.33	1120	0.40	1.00	0.00	8.96
2	50-year	415.15	8.00	0.80	0.58	285	0.70	1.00	0.07	3.99
3	50-year	1655.12	0.00	0.70	0.33	101	0.40	1.00	0.00	0.81
4	50-year	911.74	0.00	0.60	0.50	10	0.40	1.00	0.00	0.08
5	50-year	231.37	0.00	0.60	0.50	23	0.70	1.00	0.00	0.32
6	50-year	612.15	0.00	0.50	0.50	30	0.40	1.00	0.00	0.24
7	50-year	2079.53	0.00	0.70	0.33	122	0.50	1.00	0.00	1.22
8	50-year	912.08	0.00	0.60	0.50	91	0.70	1.00	0.00	1.28
9	50-year	8154.58	13.00	0.60	0.58	787	0.50	1.00	0.09	7.87
10	50-year	2612.72	73.00	0.80	0.58	1690	0.70	1.00	0.68	23.66
11	50-year	2112.54	6.00	0.80	0.58	302	0.50	1.00	0.06	3.02
12	50-year	272.99	0.00	0.60	0.50	27	0.70	1.00	0.00	0.38
13	50-year	2482.54	4.00	0.80	0.58	212	0.50	1.00	0.04	2.12
14	50-year	1798.76	3.00	0.60	0.33	50	0.50	1.00	0.01	0.50
15	50-year	1435.86	0.00	0.90	0.50	1250	0.90	1.00	0.00	22.50
16	50-year	2421.11	0.00	0.70	0.33	146	0.70	1.00	0.00	2.04
17	50-year	710.51	12.00	0.60	0.50	30	0.40	1.00	0.07	0.24
18	50-year	1639.73	0.00	0.90	0.50	1500	0.90	1.00	0.00	27.00
19	50-year	7628.64	0.00	0.70	0.33	467	0.50	1.00	0.00	4.67
20	50-year	5654.10	0.00	0.50	0.33	10	0.30	1.00	0.00	0.06
21	50-year	9433.71	0.00	0.00	0.00	10	0.00	1.00	0.00	0.00
22	100-year	1758.44	20.00	0.60	0.50	80	0.40	1.00	0.06	0.32
23	100-year	1156.55	0.00	0.90	0.50	1250	0.90	1.00	0.00	11.25
24	100-year	3023.76	0.00	0.70	0.33	183	0.70	1.00	0.00	1.28
25	100-year	3056.90	0.00	0.00	0.00	0	0.00	1.00	0.00	0.00
26	100-year	5543.71	0.00	0.50	0.33	200	0.50	1.00	0.00	1.00
27	100-year	907.19	0.00	0.60	0.50	57	0.70	1.00	0.00	0.40

Table 9. Risk grading standard of the Boshuigou debris flow.

Risk Grade (R)		Annual Probability of Personnel Loss (p)			
		$p > 0.1$	$0.01 < p \leq 0.1$	$0.001 < p \leq 0.01$	$p \leq 0.001$
Annual probability of property loss	R > 150	Very high	Very high	Very high	Very high
	50 < R ≤ 150	Very high	High	High	High
	10 < R ≤ 50	Very high	High	Medium	Medium
	R ≤ 10	Very high	High	Medium	Low

Table 10. Hazard grade and risk grade of all units.

NO	Recurrence Period	Area (m^2)	Annual Probability of Personnel Loss	Annual Probability of Property Loss	Hazard Grade	Risk Grade
1	50-year	59,962.93	0.00	8.96	high	low
2	50-year	415.15	0.07	3.99	high	medium
3	50-year	1655.12	0.00	0.81	medium	low
4	50-year	911.74	0.00	0.08	medium	low
5	50-year	231.37	0.00	0.32	medium	low
6	50-year	612.15	0.00	0.24	medium	low
7	50-year	2079.53	0.00	1.22	medium	low
8	50-year	912.08	0.00	1.28	medium	low
9	50-year	8154.58	0.09	7.87	medium	high
10	50-year	2612.72	0.68	23.66	low	very high
11	50-year	2112.54	0.06	3.02	low	high
12	50-year	272.99	0.00	0.38	medium	low
13	50-year	2482.54	0.04	2.12	medium	high
14	50-year	1798.76	0.01	0.50	medium	medium
15	50-year	1435.86	0.00	22.50	medium	medium
16	50-year	2421.11	0.00	2.04	low	low
17	50-year	710.51	0.07	0.24	low	high
18	50-year	1639.73	0.00	27.00	low	medium
19	50-year	7628.64	0.00	4.67	low	low
20	50-year	5654.10	0.00	0.06	medium	low
21	50-year	9433.71	0.00	0.00	low	low
22	100-year	1758.44	0.06	0.32	low	high
23	100-year	1156.55	0.00	11.25	low	medium
24	100-year	3023.76	0.00	1.28	low	low
25	100-year	3056.90	0.00	0.00	low	low
26	100-year	5543.71	0.00	1.00	low	low
27	100-year	907.19	0.00	0.40	low	low

The total area of the flow path and deposition is approximately 0.129 km^2. The area at very high risk is approximately 0.0026 km^2, which accounts for 2.03% of the total area; the area at high risk is approximately 0.0152 km^2, which accounts for 11.80% of the total area; the area at medium risk is approximately 0.0065 km^2, which accounts for 5.00% of the total area; the area at low risk is approximately 0.1046 km^2, which accounts for 81.17% of the total area. On this base, the risk zonation can be obtained (Figure 11). The area at very high risk appears in unit 10, which is located right side of the Boshuigou flow path, and the near residential area is at very high risk. Units 9, 11, 13, 17, and 22 are at high risk, and sparsely distributed constructions in these units are in danger; the area around the highway (G75) where units 14, 15, 18, and 23 are located is at medium risk; the other area is at low risk.

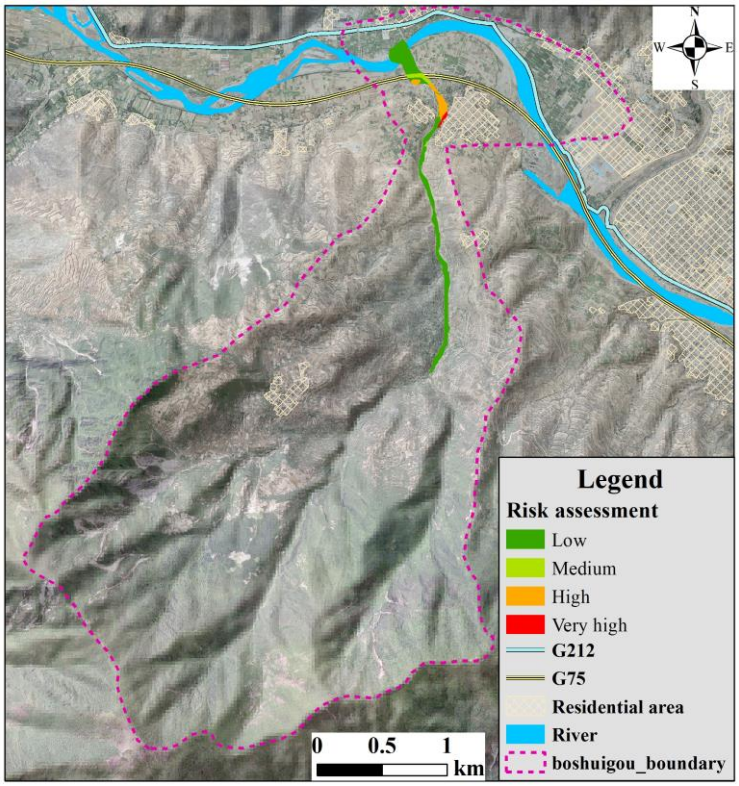

Figure 11. Risk assessment and zonation of the Boshuigou debris flow.

6. Discussion and Conclusions

For the occurrence of debris flow, sufficient loose source is the basic and necessary condition. The regional tectonic activity and widely outcropped phyllite and slate provide a large amount of loose material. In addition, steep topography at the source area and a "V"-shaped valley due to the strong down-cutting at the flow path enhances the outburst of debris flow. The frequent occurrence of the debris flow threatens the Dabao Village and highway at the deposition fan. In this light, quantity assessment of the runout and risk of the Boshuigou debris flow were performed based on detailed field investigation and numerical simulation.

Based on the simulation results of the Boshuigou debris flow under different rainfall conditions, it can be concluded that the flow depth, flow velocity, and runout distance are positively correlated with the rainfall amount. The flow process and deposition feature are controlled by the topography. Due to the flat topography near the Bailong River, the debris flow shows fan-shaped deposition for both return-period rainfall conditions. Although the deposition of the Boshuigou debris flow under the 50-year return-period rainfall reaches the Bailong River, there is a slight possibility for river damming considering its thin deposition. Much attention should be paid to the residents and constructions near the flow path. Meanwhile, the simulation result of the Boshuigou debris flow under the 100-year return-period rainfall indicate that there is a high possibility for river damming once the debris flow was triggered under this rainfall condition, as more than half the width of the Bailong River is affected by the deposition with between 0.5 and 2.5 m. Since no construction was constructed in the river, the risk assessment of the Bailong River is low.

Considering that the area flow path and the deposition area are densely populated, the corresponding hazard assessment, vulnerability assessment, and risk assessment were performed successively to accurately assess the potential destruction resulting from the debris flow. The risk assessment incorporating the construction and population, as well as their temporal and spatial probability, indicates that 13.83% of the total flow area and deposition area is at high risk, and residents in the area may be severely affected by a debris

flow outburst in the future. Based on the investigation of this work, monitoring equipment and an early warning system should be set up for this debris flow to effectively reduce the possible dam resulting from the Boshuigou debris flow.

Author Contributions: S.Z. and P.S. drafted the manuscript; Y.Z. conducted the field investigation; S.Z, J.R., and H.W. conducted the simulation and risk assessment. All authors have read and agreed to the published version of the manuscript.

Funding: This work was financially supported by the National Natural Science Foundation of China (grant number 42130720), the Fundamental Science Foundation of Institute of Geomechanics (grant number DZLXJK202007), and the China Geological Survey (DD20221738).

Institutional Review Board Statement: Not applicable.

Informed Consent Statement: Patient consent was waived.

Data Availability Statement: The data presented in this study are all available on request.

Acknowledgments: The authors are grateful for the endeavor devoted by the editor and reviewers, and their useful comments and advice are highly appreciated.

Conflicts of Interest: The authors declare no conflict of interest.

References

1. Fiorillo, F.; Wilson, R.C. Rainfall induced debris flows in pyroclastic deposits, Campania (southern Italy). *Eng. Geol.* **2004**, *75*, 263–289. [CrossRef]
2. Lu, G.Y.; Chiu, L.S.; Wong, D.W. Vulnerability assessment of rainfall-induced debris flows in Taiwan. *Nat. Hazards* **2007**, *43*, 223–244. [CrossRef]
3. Zhang, N.; Matsushima, T. Simulation of rainfall-induced debris flow considering material entrainment. *Eng. Geol.* **2016**, *214*, 107–115. [CrossRef]
4. Ietto, F.; Perri, F. Flash flood event (October 2010) in the Zinzolo catchment (Calabria, southern Italy). *Rend. Online Soc. Geol. Ital.* **2015**, *35*, 170–173. [CrossRef]
5. John, C.K.; Pu, J.H.; Pandey, M.; Moruzzi, R. Impacts of sedimentation on rainwater quality: Case study at Ikorodu of Lagos, Nigeria. *Water Supply* **2021**, *21*, 3356–3369. [CrossRef]
6. John, C.K.; Pu, J.H.; Moruzzi, R.; Pandey, M. Health-risk assessment for roof-harvested rainwater via QMRA in Ikorodu area, Lagos, Nigeria. *J. Water Clim. Chang.* **2021**, *12*, 2479–2494. [CrossRef]
7. Sepulveda, S.A.; Rebolledo, S.; McPhee, J.; Lara, M.; Cartes, M.; Rubio, E.; Silva, D.; Correia, N.; Vasquez, J.P. Catastrophic, rainfall-induced debris flows in Andean villages of Tarapaca, Atacama Desert, northern Chile. *Landslides* **2014**, *11*, 481–491. [CrossRef]
8. DeGraff, J.V.; Wagner, D.L.; Gallegos, A.J.; DeRose, M.; Shannon, C.; Ellsworth, T. The remarkable occurrence of large rainfall-induced debris flows at two different locations on July 12, 2008, Southern Sierra Nevada, CA, USA. *Landslides* **2011**, *8*, 343–353. [CrossRef]
9. García-Delgado, H.; Machuca, S.; Medina, E. Dynamic and geomorphic characterizations of the Mocoa debris flow (March 31, 2017, Putumayo Department, southern Colombia). *Landslides* **2019**, *16*, 597–609. [CrossRef]
10. Zhang, S.; Wang, F.; Li, R. First insight into the catastrophic Atami debris flow induced by a rain gush on 3 July 2021 in Shizuoka, Japan. *Landslides* **2022**, *19*, 527–532. [CrossRef]
11. Xiao, H.; Luo, Z.; Niu, Q.; Chang, J. The 2010 Zhouqu mudflow disaster: Possible causes, human contributions, and lessons learned. *Nat. Hazards* **2013**, *67*, 611–625. [CrossRef]
12. Zhai, Z.H.; Shen, W.; Li, T.L.; Zhang, Z.H.; Yin, X.D.; Zhang, G.W. Analysis and simulation of the landslide-debris flow hazard in Dagou village, Tianshui city. *J. Eng. Geol.* **2017**, *25*, 400–406.
13. Li, Y.; Chen, J.; Li, Z.; Han, X.; Zhai, S.; Li, Y.; Zhang, Y. A case study of debris flow risk assessment and hazard range prediction based on a neural network algorithm and finite volume shallow water flow model. *Environ. Earth Sci.* **2021**, *80*, 275. [CrossRef]
14. Hou, S.; Cao, P.; Li, A.; Chen, L.; Feng, Z.; Liu, J.; Wang, L. Debris flow hazard assessment of the Eryang River watershed based on numerical simulation. *Hydrogeol. Eng. Geol.* **2021**, *48*, 143–151. [CrossRef]
15. Giannecchini, R.; Naldini, D.; Avanzi, G.D.A.; Puccinelli, A. Modelling of the initiation of rainfall-induced debris flows in the Cardoso basin (Apuan Alps, Italy). *Quat. Int.* **2007**, *171*, 108–117. [CrossRef]
16. Zhou, J.W.; Cui, P.; Yang, X.G.; Su, Z.M.; Guo, X.J. Debris flows introduced in landslide deposits under rainfall conditions: The case of Wenjiagou gully. *J. Mt. Sci.* **2013**, *10*, 249–260. [CrossRef]
17. Hu, W.; Xu, Q.; Van Asch, T.W.J.; Zhu, X.; Xu, Q.Q. Flume tests to study the initiation of huge debris flows after the Wenchuan earthquake in SW China. *Eng. Geol.* **2014**, *182*, 121–129. [CrossRef]

18. Li, Q.; Huang, D.; Pei, S.; Qiao, J.; Wang, M. Using Physical Model Experiments for Hazards Assessment of Rainfall-Induced Debris Landslides. *J. Earth Sci.* **2021**, *32*, 1113–1128. [CrossRef]
19. Zhang, F.; Zhang, L.; Zhou, J. Risk assessment of debris flow in Ruoru Village, Tibet Based on FLO-2D. *J. Water Resour. Water Eng.* **2019**, *30*, 95–102.
20. Ouyang, C.; Wang, Z.; An, H.; Liu, X.; Wang, D. An example of a hazard and risk assessment for debris flows—A case study of Niwan Gully, Wudu, China. *Eng. Geol.* **2019**, *263*, 105351. [CrossRef]
21. Lee, D.H.; Lee, S.R.; Park, J.Y. Numerical simulation of debris flow behavior at Mt. Umyeon using the DAN3D model. *J. Korean Soc. Hazard Mitig.* **2019**, *19*, 195–202. [CrossRef]
22. Cesca, M.; D'Agostino, V. Comparison between FLO-2D and RAMMS in debris-flow modelling: A case study in the Dolomites. *WIT Trans. Eng. Sci.* **2008**, *60*, 197–206.
23. O'Brien, J.D. *FLO-2D User's Manual*; Version 2007.06; FLO Engineering: Nutrioso, AZ, USA, 2007.
24. Erena, S.H.; Worku, H.; De Paola, F. Flood hazard mapping using FLO-2D and local management strategies of Dire Dawa city, Ethiopia. *J. Hydrol. Reg. Stud.* **2018**, *19*, 224–239. [CrossRef]
25. Kim, S.; Paik, J.; Kim, K.S. Run-out modeling of debris flows in Mt. Umyeon using FLO-2D. *KSCE J. Civ. Environ. Eng. Res.* **2013**, *33*, 965–974.
26. Calligaris, C.; Boniello, M.A.; Zini, L. Debris flow modelling in Julian Alps using FLO-2D. *WIT Trans. Eng. Sci.* **2008**, *60*, 81–88.
27. He, P.; Wang, X.; Song, C.; Wang, Q.; Deng, L.; Zhong, S. Cenozoic evolution of the Western Qinling Mt. Range based on thermochronologic and sedimentary records from the Wudu Basin, NE Tibetan Plateau. *J. Asian Earth Sci.* **2017**, *138*, 484–494. [CrossRef]
28. Zhao, B.; Wang, Y.; Chen, M.; Luo, Y.; Liang, R.; Li, J. Typical characteristics of large-scale landslides in the transition belt between the Qinghai-Tibet Plateau and the Loess Plateau. *Arab. J. Geosci.* **2019**, *12*, 470. [CrossRef]
29. Yang, X.; Dong, Y.; Xiang, L.; Feng, Y.; Liu, D.; Luo, L.; Sun, J.; Li, D.; Li, X.; Shen, N.; et al. Two phases of Cenozoic deformation in the Wudu Basin, West Qinling (Central China): Implications for outward expansion of the Tibetan Plateau. *J. Asian Earth Sci.* **2022**, *229*, 105152. [CrossRef]
30. Chang, M.; Tang, C.; Van Asch, T.W.J.; Cai, F. Hazard assessment of debris flows in the Wenchuan earthquake-stricken area, South West China. *Landslides* **2017**, *14*, 1783–1792. [CrossRef]
31. Chang, M.; Liu, Y.; Zhou, C.; Che, H. Hazard assessment of a catastrophic mine waste debris flow of Hou Gully, Shimian, China. *Eng. Geol.* **2020**, *275*, 105733. [CrossRef]
32. Kim, T.Y.; Yun, H.S.; Kwon, J.H. A Study on the Debris Flow Hazard Mapping Method using SINMAP and FLO-2D. *J. Korean Soc. Geospat. Inf. Syst.* **2016**, *24*, 15–244. [CrossRef]
33. Zhang, P.; Ma, J.; Shu, H.; Han, T.; Zhang, Y. Simulating debris flow deposition using a two-dimensional finite model and Soil Conservation Service-curve number approach for Hanlin gully of southern Gansu (China). *Environ. Earth Sci.* **2015**, *73*, 6417–6426. [CrossRef]
34. Li, T.; Lee, G.; Kim, G. Case Study of Urban Flood Inundation—Impact of Temporal Variability in Rainfall Events. *Water* **2021**, *13*, 3438. [CrossRef]
35. Stancanelli, L.M.; Foti, E. A comparative assessment of two different debris flow propagation approaches—Blind simulations on a real debris flow event. *Nat. Hazards Earth Syst. Sci.* **2015**, *15*, 735–746. [CrossRef]
36. O'Brien, J.S. Physical Process, Rheology and Modeling of Mudflows. Ph.D. Thesis, Colorado State University, Fort Collins, CO, USA, 1986; p. 172.
37. O'Brien, J.S.; Julien, P.Y. Laboratory Analysis of Mudflow Properties. *J. Hydraul. Eng.* **1988**, *114*, 877. [CrossRef]
38. Julien, P.Y.; O'Brien, J.S. Dispersive and turbulent stresses in hyperconcentrated sediment flows. 1998; *unpublished paper*.